Applied Thermal Engineering 113 (2017) 1242–1249

Contents lists available at ScienceDirect

Applied Thermal Engineering

journal homepage: www.elsevier.com/locate/apthermeng

Research Paper

Thermal characterization of a new differential thermal expansion heat switch for space optical remote sensor

Liang Guo *, Xusheng Zhang, Yong Huang, Richa Hu, Chunlong Liu

Changchun Institute of Optics, Fine Mechanics and Physics, Chinese Academy of Sciences, Changchun, Jilin 130033, China

HIGHLIGHTS

- It is a new passively actuated differential thermal expansion heat switch for CCD.
- Automatic adjusting function decreases difficulty of manufacture and assembly.
- Good operational stability and high ratio of effective thermal resistance.
- A fairly good agreement between theoretical analysis and experiment results.

ARTICLE INFO

Article history:
Received 18 September 2016
Revised 12 November 2016
Accepted 13 November 2016
Available online 17 November 2016

Keywords:
Heat switch
Differential thermal expansion
Thermal resistance
Space optics
Thermal control

ABSTRACT

Thermal control for Charge Converse Device (CCD) is a key issue in space optical remote sensor. Heat switch is appropriate for heat dissipation of CCD. This paper provides thermal characterization of a new passively actuated differential thermal expansion heat switch (DTE-HS) with automatic adjusting function for CCD thermal control in space optical remote sensor. The radiation thermal resistance is developed to study how the radiation parameters affect the thermal resistance of the heat switch. The heat conduction thermal resistance is developed to describe the thermal characterization of the DTE-HS. A prototype of the DTE-HS is manufactured and tested. The experimental results are consistent well with the theoretical results.

1. Introduction

Space heat switch (SHS) or Space heat valve (SHV) is the device that present variable thermal resistance for thermal control. A heat switch, or heat valve, is designed to control heat transfer by making and breaking thermal contact between two contacts. In designing the heat switch, thermal resistance is the fundamental parameter of interest. Fig. 1 illustrates one possible realization of a heat switch [1]. The off state of the switch occurs when the two surfaces A and B are not in contact. The off state thermal resistance of the switch is determined by the thermal properties of the gap. The on state of the switch occurs when the two surfaces A and B are in contact. The on state thermal resistance of the switch is determined by the thermal properties of the contacts used in the switch material.

The Fig. 1 is important to characterize the performance of such a heat switch: the ratio of effective thermal resistance in the switch off and the switch on states, i.e., $\gamma_{switch} = R_{off}/R_{on}$, and the time required to switch from the off to the on state, τ_{switch}. A high thermal resistance, R_{off}, is required in the off position, so that the switch does not leak heat. A low thermal resistance, R_{on}, is required in the on position, so that the heat transfer through the switch may be maximized. Both the time to actuate the heat switch and the thermal capacitance of the switch control the switch time constant.

At present, many different heat switch configurations have been developed for space applications over the last five decades. Space heat switch species are listed in Table 1. Each configuration is based on different working principles, but most of them were developed for applications in cryogenic systems of satellites. The active heat switches are actively actuated, i.e., they require external energy to operate.

The differential thermal expansion heat switches (DTE-HSs) are based on the differential thermal expansion of distinct materials. The DTE-HSs are passively actuated, which means that they do not require external energy to operate. There are many structure distinction between heat switches which based on the same working principle. At present, there are two kinds of structures, one is

* Corresponding author.
E-mail address: guoliang329@hotmail.com (L. Guo).

http://dx.doi.org/10.1016/j.applthermaleng.2016.11.102
1359-4311/

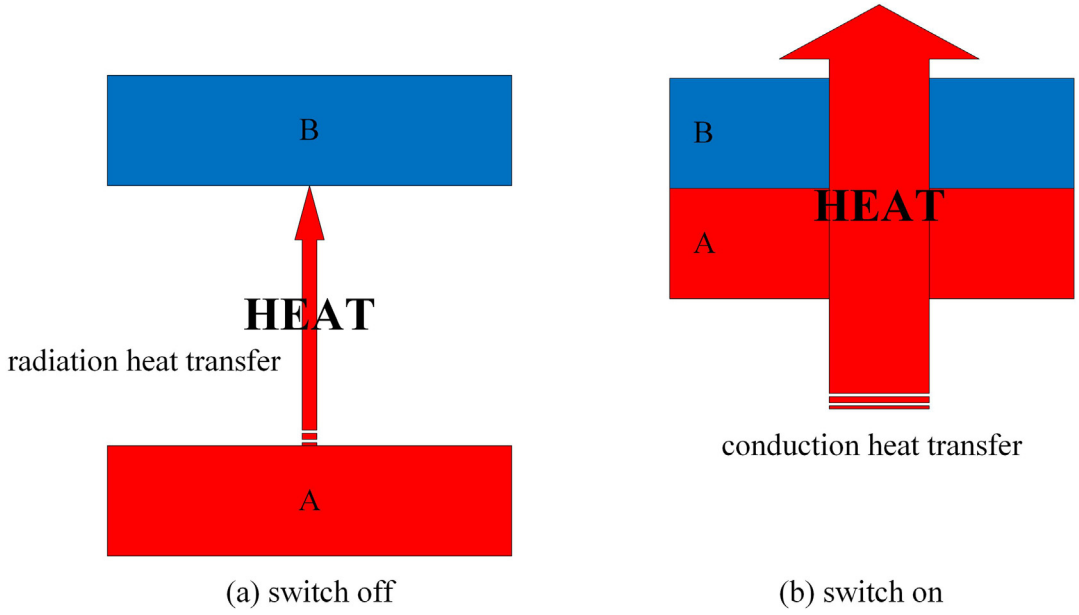

Fig. 1. Heat switch conception.

Table 1
Space heat switch configurations.

Configuration	Heat switch
Passive actuated	Bi-metallic actuated [2,3] Single direction differential thermal expansion [4,5] Double direction differential thermal expansion [6,7] Wax actuated [8–10] Shape memory alloy actuated [11,12] Pyromagnetic [13]
Active actuated	Electrostatic actuated [14–17] Piezoelectric actuated [18] Magnetic actuated [19,20] Gas-gap [21–23] Liquid bridge [24,25] EWOD actuated [26,27] Magnetoresistive [28,29] CPL/LHP [30,31]

single direction differential thermal expansion heat switch and another is double direction differential thermal expansion heat switch. The cryogenic thermal switch (CTSW) is a single direction differential thermal expansion heat switch, which is proposed by Marland et al. [4] and by Wang et al. [5] have been initially developed to couple the instrument to cryogenic systems. Two generation CTSW were developed. The first generation CTSW is made of beryllium and stainless steel. The second generation CTSW is made of polymer and aluminum. The double direction differential thermal expansion heat switch proposed by Fernando and Marcia [6] and by Zhang [7] are both used in cryogenic systems. The double direction differential thermal expansion heat switch consists of two nuts, a threaded flexible rod and a disk. The disk is placed between the nuts. The flexible rod is made of a low thermal expansion coefficient material, and the disk is made of a high thermal expansion coefficient material. One nut is fixed to the satellite structure and the other to the cryogenic sensor.

The operation temperature of Charge Converse Device (CCD) in space optical remote sensor is usually between 273 and 313 K. Most of the heat switch mentioned above are used in the cryogenic field. The operation temperature of the heat switches are between 0.1 and 100 K, which are unsuited for CCD thermal control in space optical remote sensor. When the space optical remote sensor is operating, a low thermal resistance is necessary between the CCD and the radiator in order to keep the CCD temperature as low as possible. In this situation, the heat switch provides a good thermal coupling between the CCD and the radiator. When the space optical remote sensor is not operating, the heat switch must disconnect the heat transfer for conserving energy. Under this circumstance, the heat switch must provide a high thermal resistance between the CCD and the radiator.

This paper provides a new differential thermal expansion heat switch with automatic adjusting function for CCD thermal control in space optical remote sensor. The characterization of the heat switch is studied. The first section reports a variety of heat switches. The second section outlines working principle of the heat switch. The third and fourth section present the theoretical analysis and the experimental results through a prototype. The final section provides the recommendation and conclusions from the study.

2. Differential thermal expansion heat switch

A schematic drawing of the new differential thermal expansion heat switch is shown in Fig. 2. It consists of a cylinder, a flexible rod and a disk. The flexible rod is made of a low thermal expansion coefficient material with low thermal conductivity. The flexible rod has automatic adjusting function through the flexible joint. The cylinder is made of a high thermal expansion coefficient material with high thermal conductivity. The disk is made of the same material as the cylinder. The flexible rod is fixed to the cylinder and the other to the disk. During assembly process there is a controlled gap between the cylinder and the disk at setting temperature. The cylinder is fixed to the CCD, and the disk is fixed to the radiator through a flex braid. The temperature of cylinder equal to the temperature of CCD when the space optical remote sensor isn't in operation. In the same time, the temperature of the disk drops to the radiator levels because of the flex braid. There will be a gap between the cylinder and the disk, and the thermal resistance of the heat switch achieves maximum. In this situation, the heat switch is "switch off" (Fig. 2(a)). The thermal expansion of the cylinder makes the cylinder and the disk beginning to contact each other. After the gap between the cylinder and the disk reaches

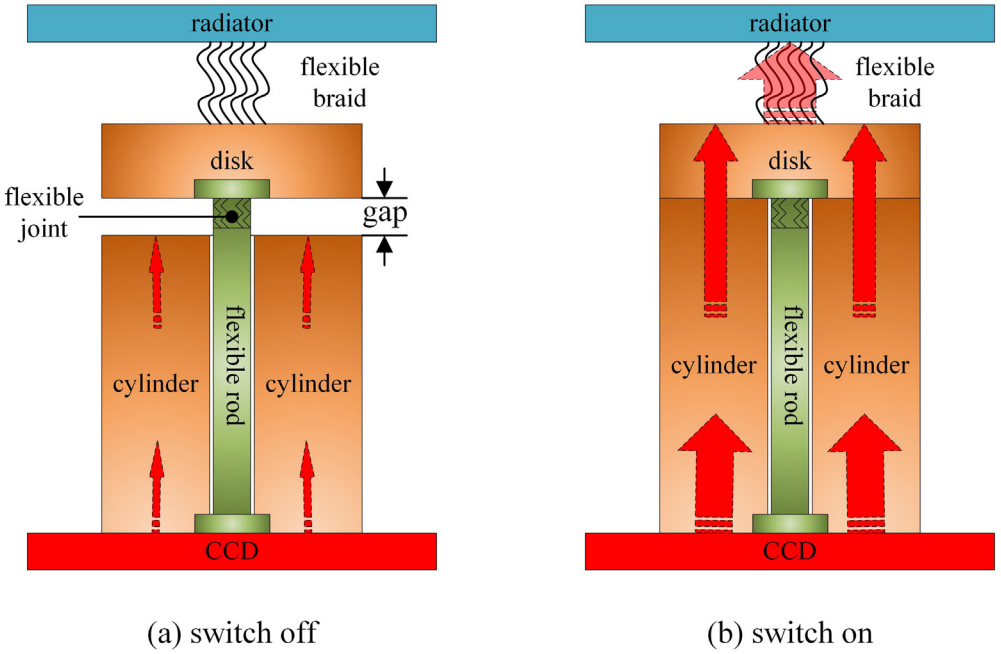

Fig. 2. Working principle of heat switch.

zero, the thermal resistance of the heat switch achieves minimum. In this situation, the heat switch is "switch on" (Fig. 2(b)). The heat load coming from the CCD to the radiator achieves maximum.

Automatic adjusting function of the flexible rod is given in Fig. 3. When the surface of cylinder (Surface C) and the surface of disk (Surface D) have a poor contact state, there will be a Δ_{gap} between the surface C and the surface D (Fig. 3(a)). The flex joint of the flexible rod will deform to adapt for improving the poor contact state between surface C and surface D (Fig. 3(b)). The flexible rod with the function of bending is not deformed by pulling or pressing in the axial direction. The thermal expansion force of the cylinder is much larger than the force required for the deformation of the flexible rod. As long as the surface C and the surface D don't contact with each other well and there is a Δgap, the thermal expansion force of the cylinder will continue to act on the disk. Because of the disk and the flexible rod are fixed together, the disk will cause the flexible rod to deform until the surface C and come into contact with the surface D well. The automatic adjusting function of the flexible rod could decrease the difficulty of manufacture and assembly of heat switch.

The prototype of the heat switch and thermal boundary conditions of the heat switch are shown in Fig. 4. The flexible rod was made of invar (4J32). The cylinder and the disk are made of aluminum alloy (2A12). Thermal conductivity of aluminum alloy (2A12) and invar (4J32) is 193 W/(m·K) and 13.5 W/(m·K) respectively.

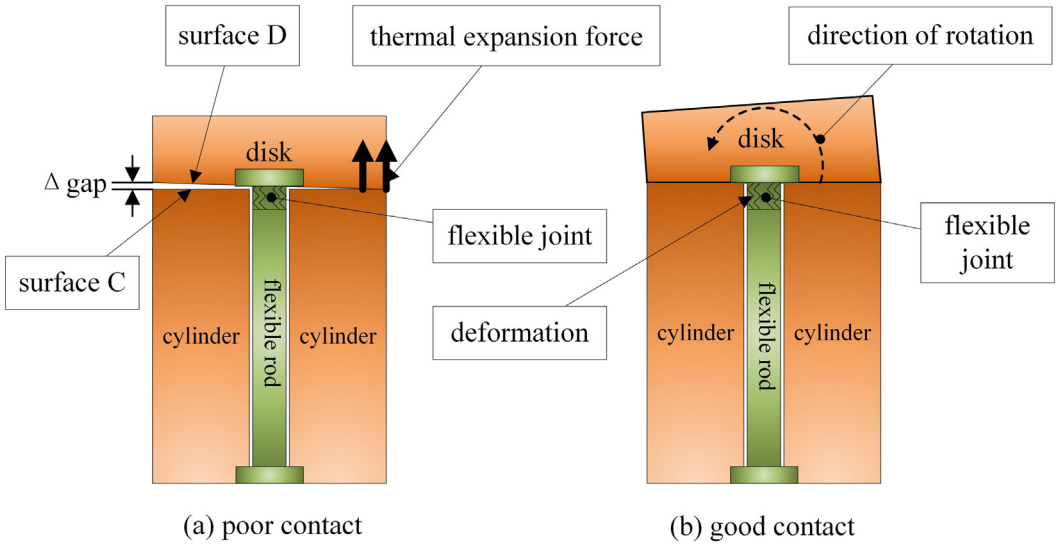

Fig. 3. Automatic adjusting function of flexible rod.

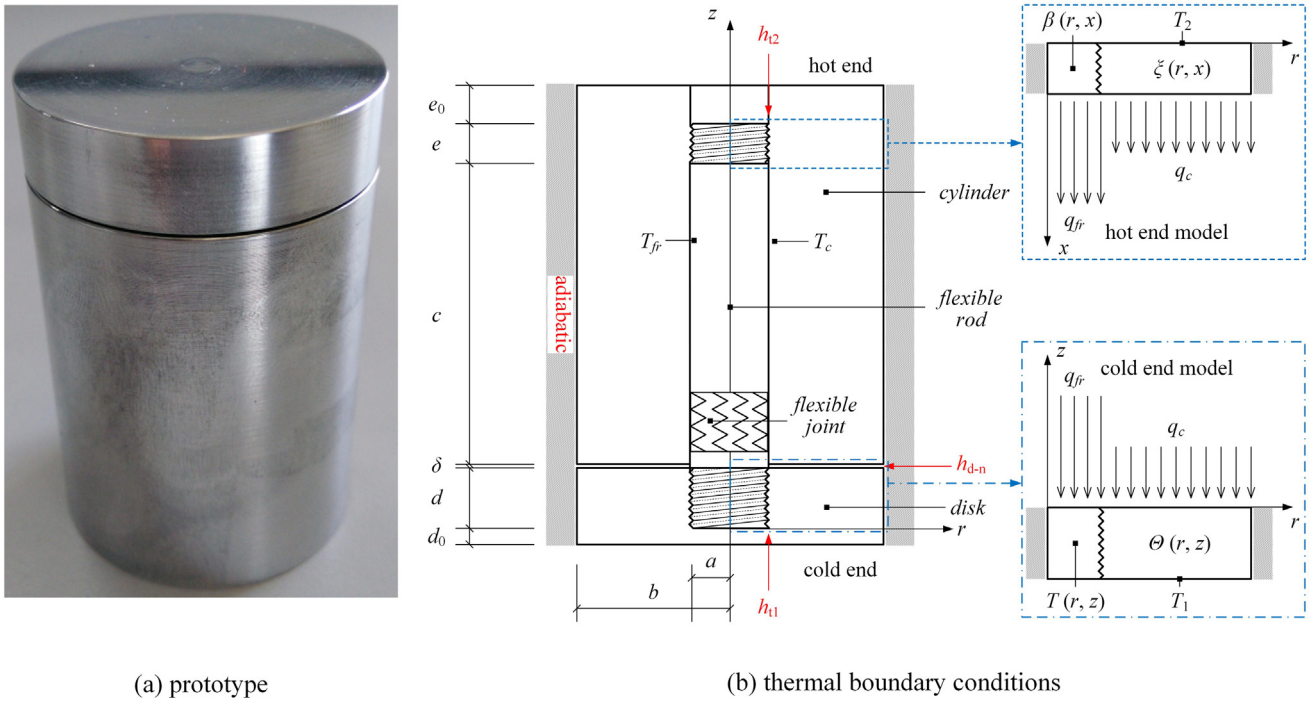

(a) prototype (b) thermal boundary conditions

Fig. 4. Prototype (a) and thermal boundary conditions (b) of the heat switch.

3. Theoretical analysis

3.1. Radiation thermal resistance

Combining the structure characteristics of the heat switch, the radiation heat transfer is concentrated in the visible surfaces of cylinder, flexible rod and disk mainly. The view factor between internal surface of cylinder and external surface of flexible rod is 1.0 approximately, the formula of surface radiation heat transfer is proposed as follows:

$$\Phi_{c-fr} = \frac{\varepsilon_c \varepsilon_{fr} A_c A_{fr} \sigma (T_c^4 - T_{fr}^4)}{\varepsilon_c A_c + \varepsilon_{fr} A_{fr} - \varepsilon_c \varepsilon_{fr} A_c} \tag{1}$$

$$R_{r,c-fr} = \frac{\Phi_{c-fr}}{T_c - T_{fr}} \tag{2}$$

In the formulas, ε_c is surface emissivity of cylinder; ε_{fr} is surface emissivity of flexible rod; A_c is internal surface area of cylinder; A_{fr} is external surface area of flexible rod; σ is blackbody radiation constant; T_c is internal surface temperature of cylinder; T_{fr} is external surface temperature of flexible rod; $R_{r,c\text{-}fr}$ is radiation thermal resistance. Obviously, radiation heat transfer is positively correlated with surface temperature difference and emissivity. From the test measurement data, the emissivity of two cylinders without polishing treatment is 0.12. Under the extreme conditions, radiation heat transfer and equivalent conduction thermal resistance is 0.013 W and 2282.2 K/W respectively.

As the annulus surface radiation heat transfer increases, R_{off} and γ_{switch} decrease simultaneously. That is, weakening the annulus surface radiation heat transfer could improve the performance of heat switch. After polishing treatment, emissivity of annulus surfaces is only 0.05. Based on the formulas of (1) and (2), radiation heat transfer and equivalent conduction thermal resistance is 0.035 W and 2542.8 K/W respectively. Above all, for the heat switch designed in this paper, radial radiation heat transfer between cylinder and flexible rod, and axial radiation heat transfer between cylinder and disk can be ignored normally, so the influences on the key thermal characteristic are not obvious extremely.

3.2. Heat conduction resistance

According to the structural characteristic of the heat switch, the heat conduction process of cylinder, flexible rod and disk can be simplified into the conduction model in cylindrical coordinates, as shown in Fig. 4.

Then, the differential equation of the two dimension, steady state and without internal heat sources heat conduction is as follow:

$$\frac{1}{r}\frac{\partial}{\partial r}(\lambda r \frac{\partial t}{\partial r}) + \frac{\partial}{\partial z}\left(\lambda \frac{\partial t}{\partial z}\right) = 0 \tag{3}$$

Considering the axisymmetric characteristic of heat switch, the temperature fields of two dimension conduction structure are assumed to $T(r,z)$ and $\Theta(r,z)$ of cold end, and $\beta(r,z)$ and $\xi(r,z)$ of hot end. Then, the differential equation of the two dimension, steady state and without internal heat sources heat conduction is as follow:

$$\begin{cases} \lambda_{fr}\left(\frac{\partial T}{\partial z}\right)_{z=d} = q_{fr} \quad 0 < r < a \\ \lambda_d\left(\frac{\partial \Theta}{\partial z}\right)_{z=d} = q_d \quad a < r < b \\ T(r,0) = T_1 + \frac{q_{fr} a}{2 h_{t1} d} \\ \Theta(r,0) = T_1 \end{cases} \tag{4}$$

$$\begin{cases} \left(\frac{\partial T}{\partial r}\right)_{r=0} = 0 \\ \left(\frac{\partial \Theta}{\partial r}\right)_{r=b} = 0 \\ \lambda_{fr}\left(\frac{\partial T}{\partial r}\right)_{r=a} = \lambda_d\left(\frac{\partial \Theta}{\partial r}\right)_{r=a} \\ -\lambda_{fr}\left(\frac{\partial T}{\partial r}\right)_{r=a} = h_{t1}[T(a,z) - \Theta(a,z)] \end{cases} \tag{5}$$

where a is locating flexible rod radius; b is heat switch external radius; c is central cylinder thickness; d_0 is initial cold end thick-

ness; d is thread cold end thickness; e_0 is initial hot end thickness; e is thread hot end thickness; δ is travelling gap between the on state and the off state; h_{t1} is thread contact thermal conductivity between locating flexible rod and the cold end; h_{t2} is thread contact thermal conductivity between flexible rod and cylinder; λ is thermal conductivity. Based on the governing equations and boundary conditions, the separation variable method is adopted to solve the temperature fields of cold end, and the calculation formulas are as follow:

$$T(r,z) = T_1 + \frac{q_{fr}a}{2h_{t1}d} + \frac{q_{fr}}{\lambda_{fr}}z + \frac{8h_{t1}d}{\pi^2}\frac{\lambda_d}{\lambda_{fr}}\left(\frac{q_{fr}}{\lambda_{fr}} - \frac{q_c}{\lambda_d}\right)\cdot\sum_{n=0}^{\infty}\frac{(-1)^n}{\Omega_n(2n+1)^2} \left\{\frac{K_1\left[\frac{\pi b}{2d}(2n+1)\right]}{I_1\left[\frac{\pi b}{2d}(2n+1)\right]} - \frac{K_1\left[\frac{\pi a}{2d}(2n+1)\right]}{I_1\left[\frac{\pi a}{2d}(2n+1)\right]}\right\} I_0\left[\frac{\pi r}{2d}(2n+1)\right]\sin\left[\frac{\pi z}{2d}(2n+1)\right] \tag{6}$$

$$\Theta(r,z) = T_1 + \frac{q_c}{\lambda_d}z + \frac{8h_{t1}d}{\pi^2}\left(\frac{q_{fr}}{\lambda_{fr}} - \frac{q_c}{\lambda_d}\right)\cdot\sum_{n=0}^{\infty}\frac{(-1)^n}{\Omega_n(2n+1)^2} \times\left\{\frac{K_1\left[\frac{\pi b}{2d}(2n+1)\right]}{I_1\left[\frac{\pi b}{2d}(2n+1)\right]} I_0\left[\frac{\pi r}{2d}(2n+1)\right] + K_0\left[\frac{\pi r}{2d}(2n+1)\right]\right\} \times\sin\left[\frac{\pi z}{2d}(2n+1)\right] \tag{7}$$

In the formulas, I_i is i order exponential growth Bessel function of first kind; K_i is i order exponential decay Bessel function of second kind. The calculation formula Ω_n is as follows:

$$\Omega_n = -\lambda_d\frac{\pi}{2d}(2n+1)\left\{\frac{K_1\left[\frac{\pi b}{2d}(2n+1)\right]}{I_1\left[\frac{\pi b}{2d}(2n+1)\right]} I_1\left[\frac{\pi a}{2d}(2n+1)\right] - K_1\left[\frac{\pi a}{2d}(2n+1)\right]\right\} + h_{t1}\left\{\frac{\lambda_d}{\lambda_{fr}}\frac{K_1\left[\frac{\pi a}{2d}(2n+1)\right]}{I_1\left[\frac{\pi a}{2d}(2n+1)\right]} I_0\left[\frac{\pi a}{2d}(2n+1)\right] + K_0\left[\frac{\pi a}{2d}(2n+1)\right]\right\} \tag{8}$$

The calculation formulas of cold end temperature field contain two unknown variables, the axial heat flux of locating flexible rod q_{fr} and the axial heat flux of cylinder q_c. Then, the concept of iso-thermal section is proposed, in where the temperature of cylinder is equal to locating flexible rod, the formula is as follow:

$$\frac{\int_0^{2\pi}\int_0^a T(r,d)rdrd\varphi}{\pi a^2} + \frac{q_{fr}(f-d)}{\lambda_{fr}} = \frac{\int_0^{2\pi}\int_a^b \Theta(r,d)rdrd\varphi}{\pi(b^2-a^2)} + \frac{q_c}{h_c} + \frac{q_c(f-d)}{\lambda_c} \tag{9}$$

After rearranging the formula, as follow:

$$\frac{2}{a^2}\int_0^a T(r,d)rdr + \frac{q_{fr}(f-d)}{\lambda_{fr}} = \frac{2}{b^2-a^2}\int_a^b \Theta(r,d)rdr + \frac{q_c}{h_c} + \frac{q_c(f-d)}{\lambda_c} \tag{10}$$

Combining the law of conservation of energy, get the following formula:

$$Q = q_{fr}\cdot\pi a^2 + q_c\cdot\pi(b^2-a^2) \tag{11}$$

The solving method of cylinder temperature fields $\beta(r,z)$ and $\xi(r,z)$ is similar to cold end, the calculation formula are as follow:

$$\beta(r,x) = T_2 - \frac{q_{fr}a}{2h_{t2}e} - \frac{q_{fr}}{\lambda_{fr}}x - \frac{8h_{t2}e}{\pi^2}\frac{\lambda_c}{\lambda_{fr}}\left(\frac{q_{fr}}{\lambda_{fr}} - \frac{q_c}{\lambda_c}\right)\cdot\sum_{n=0}^{\infty}\frac{(-1)^n}{\Gamma_n(2n+1)^2} \times\left\{\frac{K_1\left[\frac{\pi b}{2e}(2n+1)\right]}{I_1\left[\frac{\pi b}{2e}(2n+1)\right]} - \frac{K_1\left[\frac{\pi a}{2e}(2n+1)\right]}{I_1\left[\frac{\pi a}{2e}(2n+1)\right]}\right\} I_0\left[\frac{\pi r}{2e}(2n+1)\right] \times\sin\left[\frac{\pi x}{2e}(2n+1)\right] \tag{12}$$

$$\xi(r,x) = T_2 - \frac{q_c}{\lambda_c}x - \frac{8h_{t2}e}{\pi^2}\left(\frac{q_{fr}}{\lambda_{fr}} - \frac{q_c}{\lambda_c}\right)\cdot\sum_{n=0}^{\infty}\frac{(-1)^n}{\Gamma_n(2n+1)^2} \times\left\{\frac{K_1\left[\frac{\pi b}{2e}(2n+1)\right]}{I_1\left[\frac{\pi b}{2e}(2n+1)\right]} I_0\left[\frac{\pi r}{2e}(2n+1)\right] + K_0\left[\frac{\pi r}{2e}(2n+1)\right]\right\} \times\sin\left[\frac{\pi x}{2e}(2n+1)\right] \tag{13}$$

In above formulas,

$$\Gamma_n = \frac{-\pi\lambda_c}{2e}(2n+1)\left\{\frac{K_1\left[\frac{\pi b}{2e}(2n+1)\right]}{I_1\left[\frac{\pi b}{2e}(2n+1)\right]} I_1\left[\frac{\pi a}{2e}(2n+1)\right] - K_1\left[\frac{\pi a}{2e}(2n+1)\right]\right\} + h_{t2}\left\{\frac{\lambda_c}{\lambda_{fr}}\frac{K_1\left[\frac{\pi a}{2e}(2n+1)\right]}{I_1\left[\frac{\pi a}{2e}(2n+1)\right]} I_0\left[\frac{\pi a}{2e}(2n+1)\right] + K_0\left[\frac{\pi a}{2e}(2n+1)\right]\right\} \tag{14}$$

Similarly, based on the iso-thermal section, the formula can be written as:

$$\frac{2}{a^2}\int_0^a \beta(r,e)rdr - \frac{q_{fr}(h-e)}{\lambda_{fr}} = \frac{2}{b^2-a^2}\int_a^b \xi(r,e)rdr - \frac{q_c(h-e)}{\lambda_c} \tag{15}$$

$$f + h = c + d + e \tag{16}$$

The heat flux of q_{fr}, q_c and the iso-thermal section location of f, h are solved using the Eqs. (10, 11, 15 and 16), the temperature fields of heat switch structure components are obtained finally.

3.3. Theoretical results

So many complicated functions are included in the solutions above, it will affect the actual engineering applications seriously.

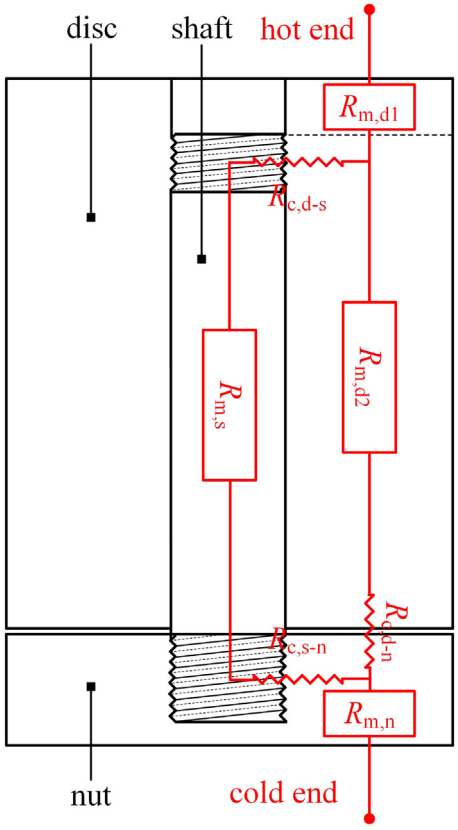

Fig. 5. One-dimensional thermal resistances network of heat switch.

Table 2
The calculation formulas of thermal resistances.

Thermal conduction resistance	(K/W)	Thermal contact resistance	(K/W)
$R_{m,c1}=\frac{e_0}{\lambda_c\cdot\pi[b^2-a^2]}$	0.02266	$R_{c,c-fr}=\frac{1}{h_{t2}\cdot 2\pi ae}$	127.324
$R_{m,c2}=\frac{e+c}{\lambda_c\cdot\pi[b^2-a^2]}$	0.19687	$R_{c,c-d}=\frac{1}{h_{c-d}\cdot\pi[b^2-a^2]}$	0.56588
$R_{m,fr}=\frac{e+c+d}{\lambda_{fr}\cdot\pi a^2}$	185.044	$R_{c,fr-d}=\frac{1}{h_{t1}\cdot 2\pi ad}$	19.2915
$R_{m,d}=\frac{(d+d_0)b^2-d_0a^2}{\lambda_d\cdot\pi b^2(b^2-a^2)}$	0.04211		

Moreover, most of the heat is conducted in the axial direction from hot end to cold end, radial heat conduction is weaker, and can be ignored absolutely. Then, the heat conduction model can be simplified into one-dimensional thermal resistance model, the one-dimensional thermal resistance network as shown in Fig. 5. Rectangles represent thermal resistances of material itself, wavy lines represent thermal contact resistances of mating surfaces, and the sum of thermal resistances in the dotted rectangle is equal to the off state thermal resistance of the switch R_{off}.

According to the relation of thermal resistances, the formulas of R_{on}^{1D}, R_{off}^{1D} and γ_{switch}^{1D} are as follows:

$$R_{on}^{1D}=R_{m,c1}+\frac{(R_{m,c2}+R_{c,c-d})\cdot(R_{c,c-fr}+R_{m,fr}+R_{c,fr-d})}{R_{m,c2}+R_{c,c-d}+R_{c,c-fr}+R_{m,fr}+R_{c,fr-d}}+R_{m,d} \tag{17}$$

$$R_{off}^{1D}=R_{m,c1}+R_{c,c-fr}+R_{m,fr}+R_{c,fr-d}+R_{m,d} \tag{18}$$

$$\gamma_{switch}^{1D}=\frac{R_{off}^{1D}}{R_{on}^{1D}} \tag{19}$$

The calculation formulas of Eq. (17-19) thermal resistances are shown in Table 2. Then, the on state thermal resistance of the switch R_{on}, the off state thermal resistance of the switch R_{off}, and the ratio of effective thermal resistance in the off and on states γ_{switch}, is 0.826 K/W, 331.7 K/W and 401.6 relatively.

4. Experimental results

4.1. Experiment set-up

The experiment set-up employed in this paper is shown in Fig. 6 (a). Laboratory temperature and relative humidity is 25 °C and 67% respectively. Experiment facilities contain electronic thermostat, KEITHLY data acquisition meter, Agilent DC power, thermostatic tank, computer and heat switch components. Meanwhile, heat switch components contain water cooling system, radiation shield, multilayer insulation blankets (MLI), thermocouples and thin film heater. The heat switch is wrapped in MLI blankets (circle and cover) to avoid thermal radiation losses to the environment. During the tests, 12 T type thermocouples located as shown in Fig. 6 (b), measured the temperatures in several points of the heat switch.

The values of thermal expansion coefficients of invar and aluminum alloy are assumed to be constant during the experiment. The elastic properties E and ν of invar and aluminum alloy are assumed to be constant during the experiment. The thermal conductivities of the invar and of the aluminum alloy were measured from cylindrical specimens machined from the same stock bars as the heat switch.

4.2. Analysis of experimental results

The temperature of heat switch were achieved at steady state condition. The thermal resistance of heat switch is given by:

$$\begin{cases} R_{switch}=\frac{T_{hot}-T_{cold}}{Q} \\ T_{hot}=\frac{T_1+T_2+T_3}{3} \\ T_{cold}=\frac{T_{10}+T_{11}+T_{12}}{3} \end{cases} \tag{20}$$

where T_{hot} and T_{cold} are the average temperatures of hot end and cold end, respectively (see Fig. 5(b)). The heat flux Q is given by:

$$Q=\eta\times V\times I \tag{21}$$

where V is the voltage and I is the current intensity of the Agilent DC power. Take into account for the heat loss from the heater to environment through the MLI blankets. The correction factor $\eta=0.7\sim0.9$ means that 10–30% of the heat dissipated from heater is leaked to the environment without crossing the heat switch.

The temperature distributions of heat switch are shown in Fig. 7 (a) and (b). There are the discontinuities between thermocouple 6 and thermocouple 7 because of the contact resistance between cylinder and disk.

From the Fig. 7(a), when the current I = 0.086 A, the correction factor $\eta=0.7$, we can obtain that the hot-cold temperature difference ΔT = 52.45 °C and the off state thermal resistance of the

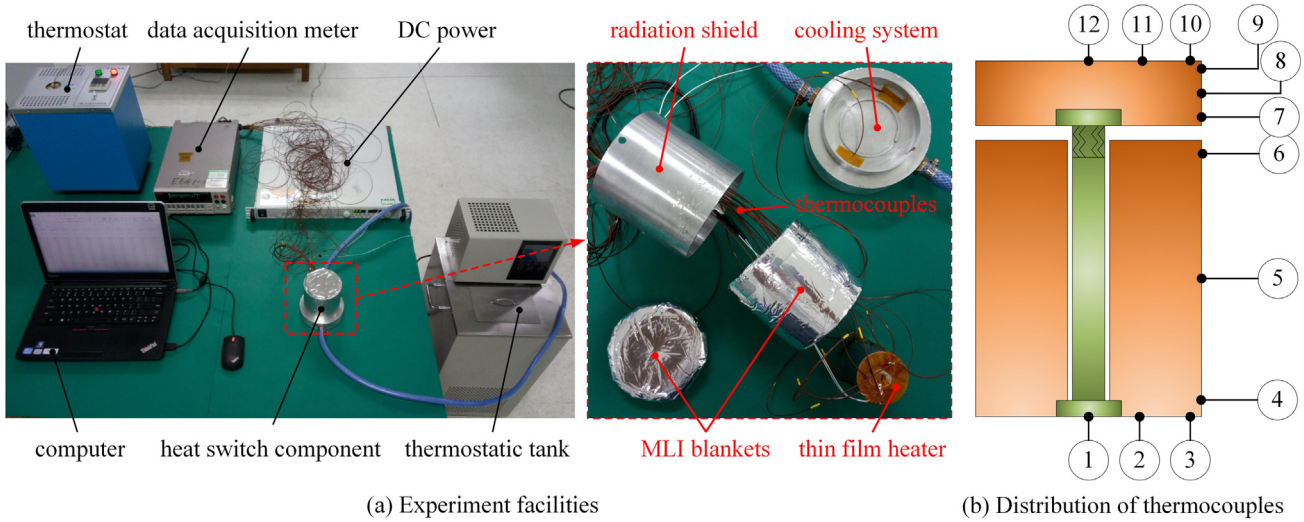

Fig. 6. Experiment set-up and distribution of thermocouples.

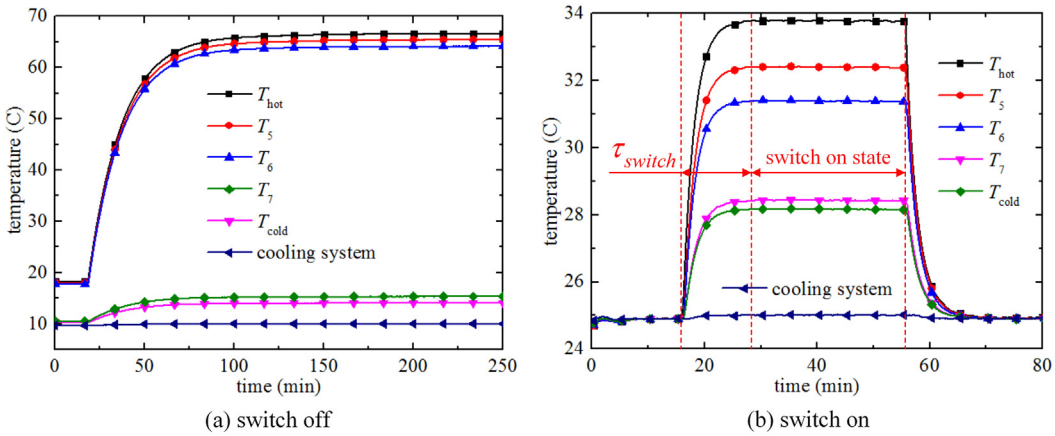

Fig. 7. Experimental results: temperature curves of switch off (a) and switch on (b).

switch, R_{off} = 316.96 K/W. The relative error between the theoretical analysis and the experiment results is 4.4%.

From the Fig. 7(b), when the current I = 0.494 A, the correction factor $\eta = 0.9$, we can obtain that the hot-cold temperature difference ΔT = 5.63 °C and the on state thermal resistance of the switch, R_{on} = 0.812 K/W. The relative error between the theoretical analysis and the experiment results is 1.7%.

Fig. 7(b) shows that the time required to switch from the off to the on state, $\tau_{switch} \approx 12$ min.

Fig. 7 shows that the ratio of effective thermal resistance in the switch off and the switch on states, $\gamma_{switch} = R_{off}/R_{on} = 390.3$. The relative error between the theoretical results and the experimental results is 2.8%.

5. Conclusions

In this study, a new differential thermal expansion heat switch with the automatic adjusting function for space optical remote sensor is modeled and analyzed. The heat switch is passively actuated through differential thermal expansion. The theoretical analysis model for thermal resistance of the heat switch were developed. A prototype of the heat switch was manufactured and an extensive experiment was performed to investigate the thermal characterization of the heat switch. The main conclusions are summarized as follows:

(a) The theoretical analysis shows that radial radiation heat transfer between cylinder and flexible rod, and axial radiation heat transfer between cylinder and disk can be ignored normally, so the influences on the key thermal characteristic are not obvious extremely. The temperature distribution of the heat switch is primarily one-dimensional along the axial direction.

(b) The one-dimensional thermal resistance model shows that the on state thermal resistance of the heat switch R_{on}, the off state thermal resistance of the heat switch R_{off}, and the ratio of effective thermal resistance in the off and on states γ_{switch}, is 0.826 K/W, 331.7 K/W and 401.6 relatively.

(c) The experiment results revealed that the on state thermal resistance of the heat switch R_{on}, the off state thermal resistance of the heat switch R_{off}, and the ratio of effective thermal resistance in the off and on states γ_{switch}, is 0.812 K/W, 316.96 K/W and 390.3 relatively. The time required to switch from the off to the on state $\tau_{switch} \approx 12$ min.

(d) The comparison between theoretical results and experimental results shows a very good agreement. The relative error of R_{off} between the theoretical analysis and the experiment results is 4.4%. The relative error of R_{on} between the theoretical analysis and the experiment results is 1.7%. The relative error of γ_{switch} between the theoretical analysis and the experiment results is 2.8%.

As a result, it was confirmed that the proposed new differential thermal expansion heat switch showed a good operational stability and a high ratio of effective thermal resistance in the off and on states. Therefore, it is expected that the heat switch can be adapted to thermal control for CCD in space optical remote sensor.

Acknowledgements

This work was supported by National Natural Science Foundation of China (Grant No. 61605203) and Youth Innovation Promotion Association of Chinese Academy of Sciences (Grant No. 2015173).

References

[1] L. Guo, X.S. Zhang, Y. Huang, et al., Application and development of space heat switch in spacecraft thermal control, Opt. Precis. Eng. 23 (1) (2015) 216–229.
[2] J.M.F. Vickers, R.R. Garipay, Thermal Design Evolution and Performance of the Surveyor Spacecraft, AIAA, No. 68-1029, 1968.
[3] F.M. Theodore, N.G. David, Development of the Viking mars lander thermal control subsystem design, J. Spacecraft 13 (4) (1968) 229–236.
[4] B. Marland, D. Bugby, C. Stouffer, Development and testing of an advanced cryogenic thermal switch and cryogenic thermal switch test bed, Cryogenics 44 (2004) 413–420.
[5] M.F. Wang, T. Yan, G.T. Hong, et al., Experimental research on a practical cryogenic heat switch, Cryogenics 2 (2006) 54–57.
[6] H.M. Fernando, B.H.M. Marcia, Theoretical and experimental studies of a bi-metallic heat switch for space applications, Int. J. Heat Mass Transf. 46 (2003) 4573–4586.
[7] L. Zhang, X.W. He, Z.H.G. Huang, et al., State-of-arts of space-borne cryogenic thermal switches, Infrared 29 (7) (2008) 15–19.
[8] S. Eric, L. Kurt, P. Mike, S. N. Keith, B. Gajanana, Wax-actuated heat switch for Mars surface applications, CP608 Space Technology and Applications International Forum-STAIF (2002), pp. 211–213.
[9] S.N. Ketith, J.P. Charles, C.B. Gajanan, et al. Development of a thermal control architecture for the Mars exploration rovers, CP654, Space Technology and Applications International Forum-STAIF, 2003, pp. 194–205.
[10] Andrew David Williams, Robust Satellite Thermal Control Using Forced Air Convection Thermal Switches for Operationally Responsive Space Missions [D] , B.S., Texas A & M University, 2002.
[11] V.B. Krishnan, Design, Fabrication and Testing of a Shape Memory Alloy Based Cryogenic Thermal Conduction Switch [D], University of Central Florida, 2004.
[12] W.Q. Zhang, Design and theoretical analyzes of shape memory alloy heat switch for spaceflight, Vacuum Cryogen. 15 (1) (2009) 41–44.
[13] Shijian Xian. Heat Switch Device: China, CN1221200 [P], 1999.
[14] M.A. Beasley, S.L. Firebaugh, R.L. Edwards, MEMS thermal switch for spacecraft thermal control [C], in: S.W. Janson, A.K. Henning, MEMS/MOEMS Components and Their Application, Bellingham, WA: Proceedings of SPIE, 2004.
[15] T. Slater, P.V. Gerwen, E. Masure, et al. Thermo-mechanical characteristics of a thermal switch [C], in: The 8th International Conference on Solid-States

Sensors and Actuators, and Eurosensors IX, Stock-holm, Sweden, June 25–29, 1995.
[16] X.Y. Wang, X.K. Chen, S.H.Z.H. Cao, et al., Thermal performance analysis of electrostatic switched radiator for satellite, Vacuum Cryogen. 15 (1) (2009) 25–29.
[17] S.H.Z.H. Cao, X.K. Chen, X.Y. Wang, et al., Novel type of micro-variable radiator for spacecraft thermal control, Vacuum Cryogen. 33 (8) (2013) 751–754.
[18] J.H. Cho, R.F. Richards, D.F. Bahr, et al., Efficiency of energy conversion by piezoelectrics, Appl. Phys. Lett. 89 (2006) 104107.
[19] C. Joshi, C. Tai, A. Mavanur, Heat Switch: US, 2005283230, 2005.
[20] Xiang Yanchao, Peng Fanghan, Shao Xingguo. Current status and research development of space heat switch technique [C], in: 8th Space Thermophysics Conference, Nanchang, Sep 2007.
[21] I. Catarino, G. Bonfait, L. Duband, Neon gas-gap heat switch, Cryogenics 48 (2008) 17–25.
[22] J. Franco, D. Martins, I. Catarino, G. Bonfait, Narrow gas gap in cryogenic heat switch, Appl. Therm. Eng. 70 (2014) 115–121.
[23] Baozhi Zhao, Qiuliang Wang, Lankai Li, et al., Practical application of gas-gap thermal switch in conduction cooled superconducting magnet system, IEEE Transac. Appl. Super-conductivity 22 (3) (2012).
[24] Su-Heon Jeong, Wataru Nakayama, Sun-Kyu Lee, Experimental investigation of a heat switch based on the precise regulation of a liquid bridge, Appl. Therm. Eng. 39 (2012) 151–156.
[25] Su-Heon Jeong, Sung-Ki Nama, Wataru Nakayama, Sun-Kyu Lee, New design of a liquid bridge heat switch to ensure repetitive operation during changes in thermal conditions, Appl. Therm. Eng. 59 (2013) 283–289.
[26] Jian Gong, Gilhwan Cha, Y. Sungtaek Ju, Thermal switches based on coplanar EWOD satellite thermal control, MEMS 1 (2008) 13–17.
[27] Aric L. Ranen McLanahan, The Design, Modeling, Fabrication, and Characterization of an EWOD Actuated Microthermal Switch, Washington State University, 2011.
[28] P.C. Ho, R.B. Hallock, A compact design for an indium heat switch, J. Low Temp. Phys. 121 (5/6) (2000) 797–802.
[29] J. Bartlett, G. Hardy, I. Hepburn, et al., Thermal characterization of a tungsten magnetoresistive heat switch, Cryogenics 50 (2010) 647–652.
[30] Yu.F. Maydanik, M.A. Chernysheva, V.G. Pastukhov, Review: loop heat pipes with flat evaporators, Appl. Therm. Eng. 67 (2014) 294–307.
[31] Valery M. Kiseev, Valeri V. Vlassov, Issamu. Muraoka, Experimental optimization of capillary structures for loop heat pipes and heat switches, Appl. Therm. Eng. 30 (2010) 1312–1319.